Spin fluctuations in γ-Fe and in Fe_3Pt Invar from local-density-functional calculations

M. Uhl, L.M. Sandratskii, and J. Kübler
Institut für Festkörperphysik, Technische Hochschule, D-64289 Darmstadt, Germany
(Received 6 January 1994)

The electronic structure and the ensuing magnetic properties of γ-Fe and Fe_3Pt Invar are determined using the local approximation to spin-density-functional theory and the augmented-spherical-wave method. A noncollinear constrained-moment procedure is described and employed to obtain the total energy as a function of the volume and the magnetic moment arranged both in collinear and noncollinear spiral structures. This, on a microscopic basis, establishes the connection between the volume with longitudinal and transverse spin fluctuations. We determine the thermal expansion coefficients of γ-Fe and Fe_3Pt and give an explanation of their anomalous magnetovolume properties.

I. INTRODUCTION

Since the time of discovery of magnetic alloys with anomalously low thermal expansion coefficients by Guillaume[1] these alloys have been subject of numerous investigations. Well-known cases are Fe_xNi_{1-x} and Fe_xPt_{1-x} for certain compositions, x; over a wide range of temperature they possess approximately invariant thermal expansion coefficients which gave rise to the name Invar. Detailed recent review papers are those given in Refs. 2–6.

To understand the Invar effect theoretically there basically have been two different approaches, one starting from the localized electron picture the other from the itinerant electron picture. Wassermann[2,3] summarized the situation in some detail. It appears that, on the basis of total-energy calculations, a consensus has recently been reached in favor of the itinerant-electron picture; early local-density-functional calculations[7,8] indicated that there are two energetically nearly degenerate states, a high-spin state (HS) with a large volume and a large magnetic moment and a low-spin state (LS) with a small volume and a small or even vanishing magnetic moment. The energy difference of these states should be in the thermal range to set up longitudinal spin fluctuations that lead to unusual magnetoelastic properties. The situation was reminiscent of the phenomenological two-state model postulated by Weiss.[9] Following these early, rather sketchy calculations, a large number of detailed calculations appeared[10–20] that provided a solid basis for the itinerant electron theory of Invar. We emphasize that in some notable cases, like for instance the calculation of Moruzzi cited in Ref. 3 and of others,[10,12,18,20] the total energies calculated as a function of the volume and the magnetic moment [in the local approximation to density-functional theory, LDA (Refs. 21 and 22)] were used as a data base for a Ginzburg-Landau theory to describe magnetovolume properties quantitatively. Initially only longitudinal magnetic fluctuations were considered in what essentially were transitions between the HS and LS states, but Wagner[11] in a phenomenological way incorporated transverse spin fluctuations, too, see also Refs. 16 and 20.

In this paper for the first time we present *ab initio* calculations for the total energy incorporating both longitudinal and transverse spin fluctuations. Our theory rests on previous developments that enable us to treat in a rather general manner noncollinear[23] magnetic states and incommensurate spin-spiral states.[24–26] Here we apply our theory to γ-Fe and to Fe_3Pt-Invar and find that transverse spin fluctuations contribute in an essential way to the formation of the Invar anomaly in Fe_3Pt; this leads to an understanding of the Invar effect that, though it relies on the existence of HS and LS states, does not require them to be near-degenerate. Thus our results yield a magnetovolume anomaly without the somewhat artificial near-degeneracy that was thought to be so essential in the previous theories. As in recent calculations for FeNi-Invar (Refs. 20 and 27) we use the nonrelativistic LDA for Fe_3Pt that, unlike relativistic calculations, results in a ferromagnetic ground state in agreement with experiment. We add that our calculations are restricted to crystallographically ordered Fe_3Pt; we thus restrict our attention to spin disorder and make no attempt to discuss effects of crystallographic disorder.

We begin in Sec. II with a brief description of the theoretical background and its implementation describing our treatment of noncollinear and spin-spiral states for arbitrary crystal structures; this generalizes our previous formulation[26] which was given for the case of an elemental metal only. We then explain in some detail how we constrain the magnetic moment in a general magnetic-moment arrangement to any desired value, m. This enables us to obtain the total energy as a function of m, of the volume and of the wave vector $\mathbf{q}$ that defines the spin spiral. In Sec. III we present results of our calculations which we use in Sec. IV to estimate finite temperature properties of γ-Fe and Fe_3Pt. In Sec. V we offer our conclusions.

II. THEORETICAL BACKGROUND

A. The Hamiltonian

The Euler-Lagrange equations that minimize the total energy as functional of the density define an effective single-particle Hamiltonian[21,22] which for spin-polarized electrons forming a noncollinear magnetic order may be written in bispinor form as[24,25]

$$\hat{\mathbf{H}}(\mathbf{r}) = -\nabla^2 \mathbf{1} + \sum_{j\nu} \mathbf{U}^{+}(\theta_{j\nu}, \phi_{j\nu})\, \mathbf{V}_{\nu}(\mathbf{r}_{j\nu})\, \mathbf{U}(\theta_{j\nu}, \phi_{j\nu}) \quad . \tag{1}$$

Here $\mathbf{U}(\theta_{j\nu}, \phi_{j\nu})$ is the standard spin-$\frac{1}{2}$-rotation matrix,

$$\mathbf{U}(\theta_{j\nu}, \phi_{j\nu}) = \begin{pmatrix} \cos(\theta_{j\nu}/2)\exp(i\phi_{j\nu}/2) & \sin(\theta_{j\nu}/2)\exp(-i\phi_{j\nu}/2) \\ -\sin(\theta_{j\nu}/2)\exp(i\phi_{j\nu}/2) & \cos(\theta_{j\nu}/2)\exp(-i\phi_{j\nu}/2) \end{pmatrix} \quad , \tag{2}$$

which describes the transformation between a global and a local spin coordinate system as defined below. Throughout we use the label j to designate the unit cell and the label ν the basis atom. The polar angles $\theta_{j\nu}$, $\phi_{j\nu}$ give the direction of the local magnetization,

$$\mathbf{m}_{j\nu} = m_{\nu} \cdot \begin{pmatrix} \cos\phi_{j\nu}\sin\theta_{j\nu} \, , & \sin\phi_{j\nu}\sin\theta_{j\nu} \, , & \cos\theta_{j\nu} \end{pmatrix} \quad , \tag{3}$$

with respect to a global coordinate system and

$$\mathbf{V}_{\nu}(\mathbf{r}_{j\nu}) = \begin{pmatrix} v_{\nu\uparrow}(\mathbf{r}_{j\nu}) & 0 \\ 0 & v_{\nu\downarrow}(\mathbf{r}_{j\nu}) \end{pmatrix} \tag{4}$$

is the spin-polarized potential of the atom at site $(j\nu)$ in the local frame of reference. The potential is unambiguously given by functional derivatives of the total energy in the local-density approximation[23] and it is centered at $\mathbf{r}_{j\nu} = \mathbf{r} - \boldsymbol{\tau}_{\nu} - \mathbf{R}_j$. Designating by $\boldsymbol{\rho}_{j\nu}$ the density matrix integrated over the atomic sphere $\Omega_{j\nu}$, i.e., $\boldsymbol{\rho}_{j\nu} = \int_{\Omega_{j\nu}} \sum_{i\in\mathrm{occ}} \boldsymbol{\psi}_i(\mathbf{r})\boldsymbol{\psi}_i^{+}(\mathbf{r}) d^3r$, where the $\boldsymbol{\psi}_i(\mathbf{r})$ are eigenstates of Eq. (1), we define the local frame of reference by those polar angles for which $\mathbf{U}(\theta_{j\nu}, \phi_{j\nu})\boldsymbol{\rho}_{j\nu}\mathbf{U}^{+}(\theta_{j\nu}, \phi_{j\nu})$ is diagonal. Here we have made an atomic-sphere approximation by averaging over the local directions in each sphere thus replacing a fine-grained mesh by the coarse-grained mesh given by the atomic spheres. When the polar angles are chosen to render the integrated density matrix diagonal we call the angles self-consistent. A particular kind of self-consistent spin configuration that we will use is given by spin spirals. Here the spin direction of each atom in the unit cell rotates around the z axis with a particular wave vector $\mathbf{q}$ which is defined by specifying the polar angles as $\theta_{j\nu} = \theta_{\nu}$, $\phi_{j\nu} = \phi_{\nu} + \mathbf{q}\cdot\mathbf{R}_j$, where θ_{ν} is restricted to special values (see Sec. II C). The spin-$\frac{1}{2}$-rotation matrices $\mathbf{U}(\theta_{j\nu}, \phi_{j\nu})$ may then be separated into an atomic contribution $\mathbf{U}(\theta_{\nu}, \phi_{\nu})$ and a lattice contribution $\boldsymbol{\Phi}(\mathbf{q}\cdot\mathbf{R}_j)$:

$$\mathbf{U}(\theta_{j\nu}, \phi_{j\nu}) = \mathbf{U}(\theta_{\nu}, \phi_{\nu})\, \boldsymbol{\Phi}(\mathbf{q}\cdot\mathbf{R}_j) \quad , \tag{5}$$

where

$$\boldsymbol{\Phi}(\mathbf{q}\cdot\mathbf{R}_j) = \begin{pmatrix} \exp(i\mathbf{q}\cdot\mathbf{R}_j/2) & 0 \\ 0 & \exp(-i\mathbf{q}\cdot\mathbf{R}_j/2) \end{pmatrix} \tag{6}$$

generates the spin transformation in the lattice of an incommensurate magnetic structure defined by $\mathbf{q}$.

Hence the Hamiltonian may be written as

$$\hat{\mathbf{H}}_{\mathbf{q}}(\mathbf{r}) = -\nabla^2 \mathbf{1} + \sum_{j\nu} \boldsymbol{\Phi}^{+}(\mathbf{q}\cdot\mathbf{R}_j)\mathbf{U}^{+}(\theta_{\nu}, \phi_{\nu})\, \mathbf{V}_{\nu}(\mathbf{r}_{j\nu}) \times \mathbf{U}(\theta_{\nu}, \phi_{\nu})\boldsymbol{\Phi}(\mathbf{q}\cdot\mathbf{R}_j) \quad . \tag{7}$$

Next we use the definition of a generalized translation operator $\{\hat{\boldsymbol{\Phi}}(\mathbf{q}\cdot\mathbf{R}_j)|\hat{T}(\mathbf{R}_j)\}$ given by Herring,[28] which combines a spin rotation $\boldsymbol{\Phi}(\mathbf{q}\cdot\mathbf{R}_j)$ [Eq. (6)] with a space translation by the vector $\mathbf{R}_j$ such that it transforms a bispinor wave function as follows:

$$\{\hat{\boldsymbol{\Phi}}(\mathbf{q}\cdot\mathbf{R}_j)|\hat{T}(\mathbf{R}_j)\}\, \boldsymbol{\psi}(\mathbf{r}) = \boldsymbol{\Phi}^{+}(\mathbf{q}\cdot\mathbf{R}_j)\, \boldsymbol{\psi}(\mathbf{r} - \mathbf{R}_j) \quad . \tag{8}$$

These generalized translations $\{\hat{\boldsymbol{\Phi}}(\mathbf{q}\cdot\mathbf{R}_j)|\hat{T}(\mathbf{R}_j)\}$ commute with the Hamiltonian and they form an Abelian group, isomorphic with the group of ordinary space translations $\{\hat{T}(\mathbf{R}_j)\}$.[24] Therefore a generalized Bloch theorem for the eigenfunctions exists which we can state as

$$\{\hat{\boldsymbol{\Phi}}(\mathbf{q}\cdot\mathbf{R}_j)|\hat{T}(\mathbf{R}_j)\}\, \boldsymbol{\psi}_{\mathbf{k}}(\mathbf{r}) = \exp(-i\mathbf{k}\cdot\mathbf{R}_j)\, \boldsymbol{\psi}_{\mathbf{k}}(\mathbf{r}) \quad . \tag{9}$$

This means that for any choice of the vector $\mathbf{q}$ it is the chemical Brillouin zone that constitutes the domain for the $\mathbf{k}$ vectors to be used for sampling the elements of the density matrix.

B. ASW implementation

Using the generalized Bloch theorem we expand the wave functions $\boldsymbol{\psi}_{\mathbf{k}}(\mathbf{r})$ in terms of the atomic bispinor functions $\phi_{\mathbf{k}\nu L\sigma}(\mathbf{r})$ in the following form:[29,30]

$$\boldsymbol{\psi}_{\mathbf{k}}(\mathbf{r}) = \sum_{\nu L\sigma} C_{\nu L\sigma}(\mathbf{k})\, \phi_{\mathbf{k}\nu L\sigma}(\mathbf{r}) \quad . \tag{10}$$

Here the coefficients $C_{\nu L\sigma}(\mathbf{k})$ are obtained by minimizing the expectation value of the Hamiltonian using the variational method.

The bispinor basis functions $\phi_{\mathbf{k}\nu L\sigma}(\mathbf{r})$ for $\mathbf{r}$ on the atomic sphere (μ) are constructed as follows:[29]

$$\phi_{\mathbf{k}\nu L\sigma}(\mathbf{r}) = h_{\nu L}(\mathbf{r}_\nu)\mathbf{U}_\nu^+\boldsymbol{\chi}_\sigma\delta_{\nu\mu} + \sum_{\nu' L'\sigma'} G^{\nu\nu'}_{LL'\sigma\sigma'}(\mathbf{k})\, j_{\nu' L'}(\mathbf{r}_{\nu'})\mathbf{U}_{\nu'}^+\boldsymbol{\chi}_{\sigma'}\delta_{\nu'\mu} \quad . \tag{11}$$

Here the quantities $h_{\nu L}(\mathbf{r}_\nu)$ and $j_{\nu' L'}(\mathbf{r}_{\nu'})$ are spherical Hankel and Bessel functions multiplied with spherical harmonics, centered at the sites (ν) and (ν'); they are solutions of the Helmholtz equation in the interstitial space with a chosen energy of -15 mRy. Inside the atomic spheres Eq. (11) has to be replaced by

$$\phi_{\mathbf{k}\nu L\sigma}(\mathbf{r}) = \tilde{h}_{\nu L\sigma}(\mathbf{r}_\nu)\mathbf{U}_\nu^+\boldsymbol{\chi}_\sigma + \sum_{\nu' L'\sigma'} G^{\nu\nu'}_{LL'\sigma\sigma'}(\mathbf{k})\, \tilde{j}_{\nu' L'\sigma'}(\mathbf{r}_{\nu'})\mathbf{U}_{\nu'}^+\boldsymbol{\chi}_{\sigma'} \quad , \tag{12}$$

where $\tilde{h}_{\nu L\sigma}(\mathbf{r}_\nu)$ and $\tilde{j}_{\nu' L'\sigma'}(\mathbf{r}_{\nu'})$ are the corresponding augmented numerical solutions of the Schrödinger equation, defined to be zero outside their respective spheres, and described in the spin-diagonal local frame of reference. The information about the orientation of the individual spin quantization axes[26] is embodied in the product of the spin-$\frac{1}{2}$-rotation matrices $\mathbf{U}$ with the bispinor basis functions $\boldsymbol{\chi}_\sigma$.

Using the Korringa-Kohn-Rostoker (KKR) expansion theorem one may expand a Hankel function at the site $(j\nu)$ in a linear combination of Bessel functions at the site $(j'\nu')$ by

$$h_{\nu L}(\mathbf{r}_{j\nu}) = \sum_{L'} B_{LL'}(\mathbf{R}_j + \boldsymbol{\tau}_\nu - \mathbf{R}_{j'} - \boldsymbol{\tau}_{\nu'})\, j_{\nu' L'}(\mathbf{r}_{j'\nu'}) \quad . \tag{13}$$

The generalized structure constants appearing in Eqs. (11) and (12) are then obtained as

$$G^{\nu\nu'}_{LL'\sigma\sigma'}(\mathbf{k}) = \left[\mathbf{U}_{\nu'}\begin{pmatrix} G^{\nu\nu'}_{LL'}(\mathbf{k}-\mathbf{q}/2) & 0 \\ 0 & G^{\nu\nu'}_{LL'}(\mathbf{k}+\mathbf{q}/2)\end{pmatrix}\mathbf{U}_\nu^+\right]_{\sigma'\sigma} \quad , \tag{14}$$

where

$$G^{\nu\nu'}_{LL'}(\mathbf{k}) = \sum_j \exp(i\mathbf{k}\cdot\mathbf{R}_j) B_{LL'}(\mathbf{R}_j + \boldsymbol{\tau}_\nu - \boldsymbol{\tau}_{\nu'}) \quad , \tag{15}$$

the quantity $B_{LL'}$ is given by a standard formula from KKR theory and may, for instance, be obtained from Eq. (16) of Ref. 26.

C. Constraining the magnetic moments

To describe the energetics of any kind of spin fluctuation it is advantageous to calculate the total energy as a function of the magnetic moment.

For a ferromagnet this was achieved in the past by the so-called fixed-spin-moment method (FSM), see, for instance, Refs. 31–33, where the energy, $E(m)$, of the state having a magnetic moment m per unit cell (uc) is obtained from a constrained variation of the form

$$E(m) = \min\left\{E[m(\mathbf{r})] + b\left(\int_{\mathrm{uc}} m(\mathbf{r})d^3r - m\right)\right\} \quad . \tag{16}$$

The Lagrange parameter b can be treated as an external magnetic field parallel to the direction of magnetization. Here the magnetization is simply obtained by adjusting two spin-dependent Fermi energies, $\varepsilon^F_\pm = \varepsilon^F \pm b$,[31] such that the resulting magnetization is equal to the desired value m.

In a general noncollinear spin structure Eq. (16) has to be replaced by

$$E(\{\mathbf{m}_\mu\}) = \min\left\{E[\mathbf{m}(\mathbf{r})] + \sum_\nu \mathbf{b}_\nu\left(\int_{\Omega_\nu}\mathbf{m}(\mathbf{r})d^3r - \mathbf{m}_\nu\right)\right\} \quad , \tag{17}$$

where on the left-hand side $\{\mathbf{m}_\mu\}$ is the set of desired moments at the sites (μ).[33,26] On the right-hand side the vector parameters $\mathbf{b}_\nu$ can be treated as magnetic fields acting on the spin densities of the corresponding atoms. The component of $\mathbf{b}_\nu$ parallel to $\mathbf{m}_\nu$ stabilizes the magnitude of the moment and the perpendicular component counteracts the torque that is produced by the nondiagonal density matrix.

In self-consistent spin arrangements the density matrix by definition is diagonal in the local frame of reference; thus in Eq. (17) the vectors $\mathbf{m}(\mathbf{r})$, $\mathbf{m}_\nu$, $\mathbf{b}_\nu$ are parallel and we may drop the vector symbols. These conditions apply to our calculations where we use planar spin spirals which are defined by $\theta_\nu = 90°$ for all sites (ν).

Thus the variation of Eq. (17) yields the following Hamiltonian:

$$\hat{\mathbf{H}}(\mathbf{r}) = -\nabla^2\mathbf{1} + \sum_{j\nu}\mathbf{U}^+(\theta_{j\nu},\phi_{j\nu})\Big(\mathbf{V}_\nu(\mathbf{r}_{j\nu}) + \boldsymbol{\sigma}^z b_\nu(\mathbf{r}_{j\nu})\Big) \times\mathbf{U}(\theta_{j\nu},\phi_{j\nu}) \quad . \tag{18}$$

Here the constraining fields [$b_\nu(\mathbf{r}_{j\nu}) = b_\nu$ inside the sphere (ν) and zero outside] must be adjusted such that the resulting moments coincide with those wanted: $\int_{\Omega_\nu} m(\mathbf{r})d^3r = m_\nu$. The Hamiltonian, Eq. (18), is not diagonal in the spin quantum numbers, a fact that leads to spin-hybridized energy bands.[26,34,35] Therefore the concept of two Fermi energies for bands with differ-

ent spin indices cannot be applied here. Thus to do the actual constrained calculations for noncollinear configurations we proceed iteratively as follows. We begin as in the FSM by using two Fermi energies for each site (ν): $\varepsilon^F_{\nu\pm} = \varepsilon^F \pm \delta_\nu$. If we start with any value b_ν, the "correction" parameter δ_ν of the corresponding local field b_ν for an arbitrary moment m_ν is given by

$$\int^{\varepsilon^F \pm \delta_\nu} N_{\nu\pm}(\varepsilon, b_\nu)\, d\varepsilon = \frac{1}{2}(n_\nu \pm m_\nu) \quad , \tag{19}$$

where the quantities $N_{\nu\pm}(\varepsilon, b_\nu)$ are the partial spin-projected densities of states of the atom (ν) in its local frame of reference obtained in the last iteration. For the next iteration the new magnetic field is assigned as

$$b_\nu^{\text{new}} = b_\nu^{\text{old}} + \delta_\nu \quad . \tag{20}$$

With Eqs. (19) and (20) the parameters b_ν are iterated to self-consistency, such that eventually $\delta_\nu = 0$ for all sites ν. This means that in the self-consistent solution one works just with a single "physical" Fermi energy $\varepsilon^F_{\nu\pm} = \varepsilon^F$. In analogy with the FSM we may call this method the noncollinear fixed-spin-moment method (NCFSM). It allows us to calculate the total energy not only as a function of the volume, but also as a function of the magnitude of the magnetic moments and for arbitrary values of the spin-spiral vector, $\mathbf{q}$.

III. RESULTS

Although the case of fcc or γ-Fe has received theoretical attention before,[26,36,37] we want to begin with this case again briefly sketching its peculiar properties and adding some new results. This will set the stage for our results concerning Fe_3Pt which we will contrast with those of γ-Fe.

A. γ-Fe

Even though the NCFSM-method allows us to carry out calculation of the total energy for an arbitrary value of the atomic moment m we will start the discussion with Fig. 1 where the results of unconstrained calculations are represented and therefore all states shown here supply an extremum of the unconstrained functional. Thus Fig. 1 shows the total energy of bcc and fcc Fe as a function of the Wigner-Seitz radius, S, in various different magnetic structures. New in this set of data is the inclusion of spiral magnetic order, whereas in all other respects it is in agreement with older work, e.g., Refs. 38–40. It should be noted that the low value of the total energy for fcc Fe compared with bcc Fe is known to be a LDA defect that disappears in a nonrelativistic calculation, see, e.g., Ref. 32. It is seen that for γ-Fe the magnetic structure depends sensitively on the volume (see also Table I).

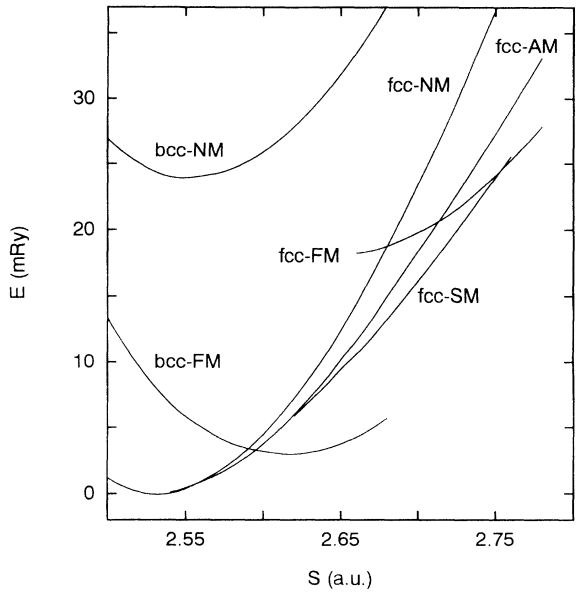

FIG. 1. Total energy per atom of γ-Fe in bcc and fcc crystal structures as a function of the Wigner-Seitz radius, S. NM, nonmagnetic; FM, ferromagnetic; AM, antiferromagnetic; and SM, spiral magnetic.

In contrast to bcc Fe, where the ground state is ferromagnetic, i.e., $\mathbf{q} = 0$,[43] in fcc Fe over a wide range of volumes the spin-spiral configuration is the state of lowest energy with a spiral vector $\mathbf{q} = (0, 0, q_z)\frac{2\pi}{a}$ close to $q_z \simeq 0.6$.[26] It occurs because, at this particular q_z, the $3d$ bands of opposite spin hybridize along the k_z axis at the Fermi energy, as was shown in detail in Ref. 26. In addition, our calculations give further locally stable configurations with $\mathbf{q} = (1, 0, 0.25)\frac{2\pi}{a}$ at $2.60 < S < 2.65$ a.u. and $\mathbf{q} = (1, 0, 0.5)\frac{2\pi}{a}$ at $2.67 < S < 2.72$ a.u., which is in agreement with neutron diffraction experiments on γ-Fe precipitates in copper.[41,42]

Using the NCFSM method described in Sec. II C we extended our calculations to arbitrary values of the local magnetic moments to obtain the total energy as a function of volume, v, the local magnetic moment, m, and magnetic structure, $\mathbf{q}$, i.e., $E(v, m, \mathbf{q})$. Our numerical experiments showed that the total energy can be written as

TABLE I. Dependency of spin configuration in γ-Fe on atomic radius and magnetic moment.

Atomic radius (a.u.)			Magnetic moment (μ_B)			Spin configuration
	S	< 2.53		m	$= 0.0$	Nonmagnetic (NM)
$2.53 <$	S	< 2.60	$0.0 <$	m	< 1.0	Antiferromagnetic (AM)
$2.60 <$	S	< 2.76	$1.0 <$	m	< 2.5	Spin-spiral magnetic (SM)
$2.76 <$	S		$2.5 <$	m		Ferromagnetic (FM)

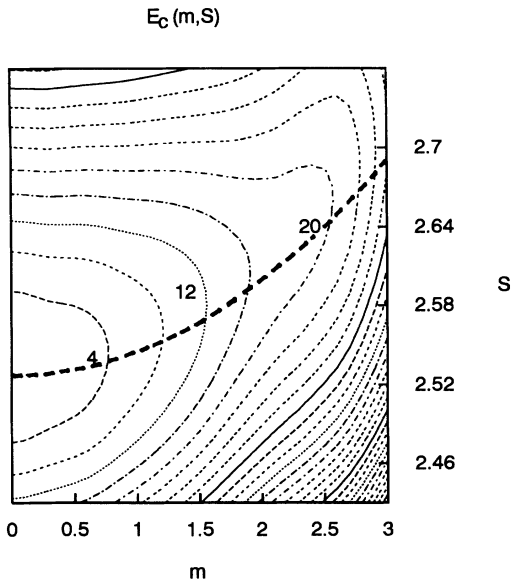

FIG. 2. Contours for γ-Fe of the collinear contribution to the total energy, E_c, see Eq. (21), in mRy per atom. S, Wigner-Seitz radius in atomic units and m, magnitude of the magnetic moment in μ_B. The locus of points defined by $\partial E_c/\partial v = 0$ is indicated by the heavy dashed line.

$$E(v, m, \mathbf{q}) = E_c(v, m) + \alpha(v) E_q(m, \mathbf{q}) \quad . \qquad (21)$$

Here $\alpha(v)$ is a slowly varying scaling factor which for the volume range investigated is $\alpha(v) \simeq (v_0/v)^4$. The first term on the right-hand side, E_c, we may call the collinear and the second, E_q, the noncollinear contribution to the total energy. We graph in Fig. 2 the collinear energy surface $E_c(v, m)$ and in Fig. 3 the noncollinear contribution $E_q(m, q_z)$.

Although all excited states contribute to the thermal properties of a crystal, these contributions depend crucially on the energy of the states decreasing rapidly with increasing energy. Therefore, to gain a qualitative understanding of temperature trends, we can concentrate on certain special features of the energy functions $E_c(v, m)$ and $E_q(m, \mathbf{q})$. Thus it is the separation of the total energy given in Eq. (21) that allows us to rather easily find the states $(v, m, \mathbf{q})$ which for a given value of the magnetic moment m minimize the total energy. Indeed, the corresponding value of $\mathbf{q}$, or here in particular q_z, can be determined by using the curve $\partial E_q/\partial q_z = 0$, see Fig. 3, and the value of v may be read off from Fig. 2 using the equality $\partial E_c/\partial v = 0$. The relation between m and q_z thus obtained is identical to that given in Table I, because in both cases they are determined by the equation $\partial E_q/\partial q_z = 0$.

B. Fe_3Pt

Fe_3Pt crystallizes in the Cu_3Au structure; it is ordered such that Pt occupies the cube corners and Fe the face centers. The atomic-sphere approximation used in our calculations requires the choice of sphere radii for the

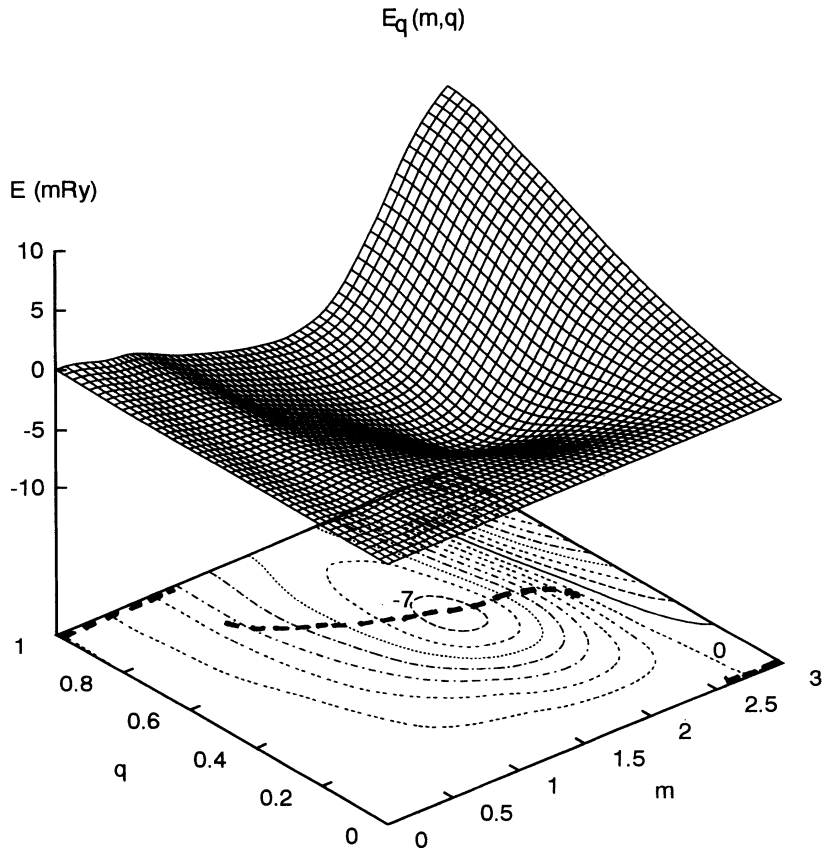

FIG. 3. Contours and surface for γ-Fe of the noncollinear contribution to the total energy, E_q, see Eq. (21), in mRy per atom. m, magnitude of the magnetic moment in μ_B and q, magnitude of the spiral vector in units of $\frac{2\pi}{a}$ along the $(0, 0, 1)$ axis. The locus of points defined by $\partial E_q/\partial q_z = 0$ is indicated by the heavy dashed line.

constituents which was such that the atomic spheres were neutral to within about 0.2 electrons per sphere. To a good approximation this leads to a minimum in the total energy at a given volume and is found to require equal sphere radii for all volumes and states of magnetic order considered.

In contrast to γ-Fe the ground state of Fe_3Pt is ferromagnetic for a sphere radius, S, of $S = 2.79$ a.u. possessing magnetic moments of $m_{Fe} = 2.67\mu_B$ and $m_{Pt} = 0.27\mu_B$. The corresponding lattice constant is $a = 3.77$ Å which is somewhat larger than the experimental lattice constant of $a = 3.73$ Å.[44] The calculated magnetic moment corresponds to $m = 2.07\mu_B$ per atom which is slightly smaller than the experimental value of $m = 2.16\mu_B$ per atom quoted by Shimizu.[45] In Fig. 4 we show the total energy per cell as a function of the Wigner-Seitz radius, S. Figure 4 differs from older calculations in a number of details (see Refs. 17 and 3); these are the numerical values of the total-energy difference between the ferromagnetic and non-magnetic states, the values of the equilibrium lattice constant and the equilibrium magnetic moment. This is so because our calculations are not relativistic in contrast to the older calculations where the scalar-relativistic wave equation (SRWE) was used. As we pointed out in the Introduction, our results are closer to experimental ground-state properties than those obtained with the SRWE. The same observation was made in Sec. III A for fcc and bcc Fe. This is our only justification for neglecting relativistic corrections here.

Continuing with the discussion of our results we notice in Fig. 4 that the spin-spiral states possess the lowest total energy for a wide range of volumes, but, in contrast to γ-Fe these states are seen to occur at volumes smaller than the calculated equilibrium volume. Furthermore, the collinear antiferromagnetic state (not shown in Fig. 4) is higher in energy than the ferromagnetic state. In particular see Table II.

A detail should be noted here. For reasons of symmetry we chose the spiral vector to be parallel to the $(1,1,1)$ axis: $\mathbf{q} = q \cdot (1,1,1)\frac{2\pi}{a}$. This leaves all three Fe positions of the Fe_3Pt unit cell magnetically and chemically equivalent. The spin-spiral magnetic order of lowest energy for a wide range of volumes of Fe_3Pt is given approximately by $q = 0.25$. This can be translated into the angle between the spins of two neighboring ferromagnetic planes to be about 90° which is close to the angle in γ-Fe of 108°.

As in the case of γ-Fe the total energy can be written as a sum of a collinear contribution, $E_c(v,m)$, and a noncollinear contribution, $E_q(m,q)$, see Fig. 5 and Fig. 6, which, as was pointed out in Sec. III A, facilitates the discussion greatly. Thus from Fig. 6 we find for a given local moment, m, the value of q corresponding to the state with the lowest total energy and from Fig. 5 the relevant value of the volume, v. Figure 6 shows that in the case of Fe_3Pt for $m > 2.6\mu_B$ the energy is lowest in ferromagnetic order and for $m < 2.6\mu_B$ the energy is minimized by a spin-spiral structure with values of q lying in the interval from 0.2 to 0.3.

For the discussion that follows it is important to note that the noncollinear portion of the total energy $E_q(m,q)$ has a clear tendency to increase for large m, see Fig. 6. In particular the noncollinear contribution, $E_q(m,q)$, is negative for states with small moments, $(m < 2.6\mu_B)$, and positive for states with large moments, $(m > 2.6\mu_B)$. Therefore, this contribution with heating leads to a preferable occupation of noncollinear states having local magnetic moments smaller than the ground-state value of $m_0 = 2.67\mu_B$ (see also Sec. IV).

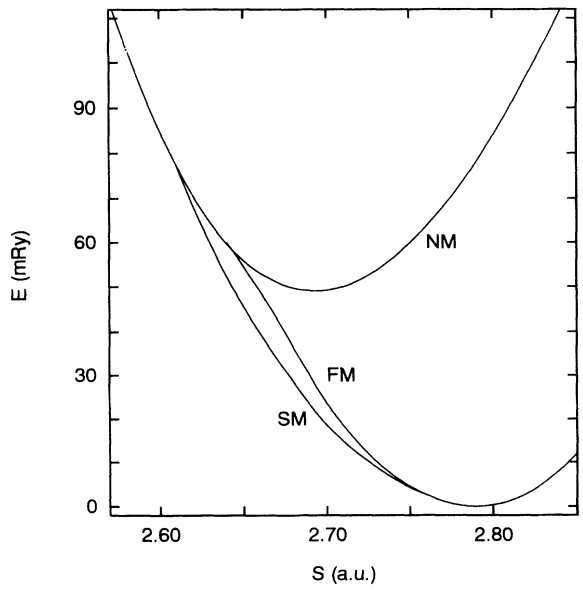

FIG. 4. Total energy per unit cell of Fe_3Pt as a function of the Wigner-Seitz radius, S. NM, nonmagnetic; FM, ferromagnetic; and SM, spiral magnetic.

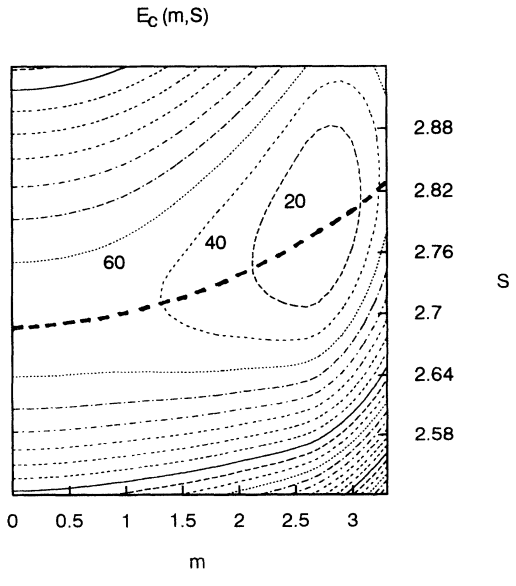

FIG. 5. Contours for Fe_3Pt of the collinear contribution to the total energy, E_c, see Eq. (21), in mRy per unit cell; S, Wigner-Seitz radius in atomic units; and m, magnitude of the magnetic moment in μ_B. The locus of points defined by $\partial E_c/\partial v = 0$ is indicated by the heavy dashed line.

TABLE II. Dependency of spin configuration in Fe_3Pt on atomic radius and magnetic moment.

Atomic radius (a.u.)			Magnetic moment (μ_B)			Spin configuration
	S	< 2.60		m	$= 0.0$	Nonmagnetic (NM)
$2.60 <$	S	< 2.76	$0.0 <$	m	< 2.6	Spin-spiral magnetic (SM)
$2.76 <$	S		$2.6 <$	m		Ferromagnetic (FM)

We may add that for the ferromagnetic ground state of Fe_3Pt our calculations give a hyperfine field for Fe of -290 kOe which is in reasonable agreement with experimental values.[44] Our calculations show a distinct tendency for a decrease of the hyperfine field when the angle between neighboring spins increases; e.g., for $q = 0.25$ the calculated hyperfine field is -200 kOe without a noticeable change in the value of the local magnetic moment.

The information on the total energy of spiral structures can be used for a rough estimate of both the Curie temperature, T_C, and the spin-wave stiffness constant, D. The Curie temperature T_C can be estimated within the mean field approximation to the Heisenberg Hamiltonian. Neglecting the magnetic contribution of platinum, the Curie temperature is given by $T_C = \frac{m_0+2}{3m_0} J(0)$. Here the exchange parameter $J(0)$ is calculated by $J(0) = \Omega_{BZ}^{-1} \int_{BZ} d^3q \Delta E(\mathbf{q})$, where $\Delta E(\mathbf{q}) = [E(v_0, m_0, \mathbf{q}) - E(v_0, m_0, 0)]/3$ is the total energy per Fe atom counted from the ground state and Ω_{BZ} is the volume of the Brillouin zone. Our calculations give $T_C = 435$ K, which is in good (probably fortuitous) agreement with the experimental value of ordered Fe_3Pt, $T_C = 430$ K.[3,46] We hasten to point out that we do not imply here the localized-electron picture is appropriate for a description of the magnetovolume effects.

To estimate the spin-wave stiffness constant D we use the following expression:[47] $D = \frac{4}{m_0} \lim_{q \to 0} \frac{\Delta E(\mathbf{q})}{|\mathbf{q}|^2}$, with $\Delta E(\mathbf{q})$ defined above, we obtain the value of $D = 135$ meV Å^2 which should be compared with the value of $D = 80$ meV Å^2 for $Fe_{72}Pt_{28}$.[3,48]

IV. DISCUSSION OF THERMODYNAMIC PROPERTIES

In this section it is our purpose to show that the information accumulated in the total-energy surfaces dis-

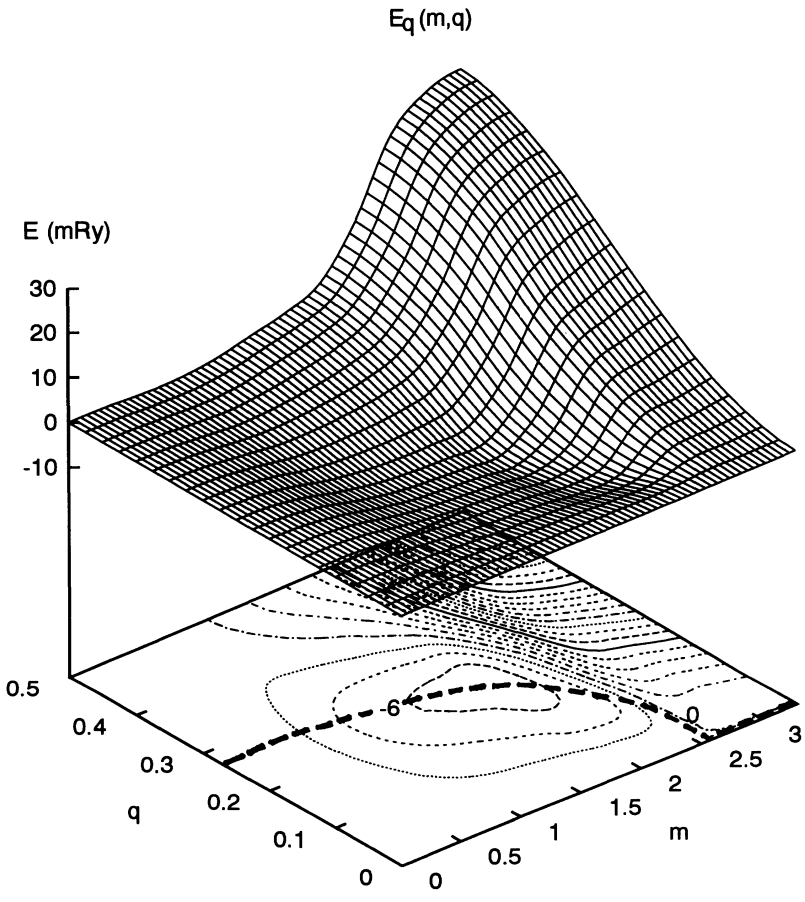

FIG. 6. Contours and surface for Fe_3Pt of the noncollinear contribution to the total energy, E_q, see Eq. (21), in mRy per unit cell. m, magnitude of the magnetic moment in μ_B and q, magnitude of the spiral vector in units of $\frac{2\pi}{a}$ along the $(1,1,1)$ axis. The locus of points defined by $\partial E_q/\partial q = 0$ is indicated by the heavy dashed line.

cussed above supplies a good description of the anomalous tendencies in the temperature variation of the specific volume. However, we do not attempt to construct a consistent statistical mechanics scheme but within a rather simple scheme for statistical averages we show that excited states modeled by noncollinear arrangement of magnetic moments give an important contribution to thermodynamic properties.

For the averaging process which we want to use here we will make use of all calculated states; therefore the phase space is parametrized by v, m, and $\mathbf{q}$. The probability function of any state is defined as

$$p(v,m,\mathbf{q};T) = f_B(v,m,\mathbf{q};T) \Big/ \left(\int D(v,m,\mathbf{q})\ f_B(v,m,\mathbf{q};T) \right) \quad , \tag{22}$$

where

$$f_B(v,m,\mathbf{q};T) = \exp(-E(v,m,\mathbf{q}) \ / \ k_B T) \tag{23}$$

is the Boltzmann factor and

$$\int D(v,m,\mathbf{q}) = \int dv \int m^2 dm \int_{\mathrm{BZ}} d^3q \tag{24}$$

denotes the integration over all three parameters. On the basis of this probability function we calculate the distribution of any variable $x(v,m,\mathbf{q})$ by

$$n_x(x_0;T) = \int D(v,m,\mathbf{q})\ p(v,m,\mathbf{q};T)\ \delta[x(v,m,\mathbf{q}) - x_0] \tag{25}$$

and its average value by

$$\langle x(T) \rangle = \int dx_0\ n_x(x_0;T)\ x_0 \quad . \tag{26}$$

As the variable x we may choose any physical quantity characterizing the crystal, in particular the specific volume, the magnitude of the local magnetic moment, or even components of $\mathbf{q}$.

The integral over q extends over the entire Brillouin zone and we integrate over fluctuations of the volume, the magnitude of the magnetic moments, and over transverse spin fluctuations. For temperatures up to about 600 K no artificial cutoff parameters are needed in these integrals, therefore the integrals pose no problems for low and intermediate temperatures. To sample the spin-wave states in the Brillouin zone we used for γ-Fe a mesh of 256 $\mathbf{q}$ vectors spread uniformly over the full Brillouin zone. For Fe_3Pt, however, we are limited presently by symmetry (see Sec. III B) and computer time to use $\mathbf{q}$ vectors along the $(1,1,1)$ axis. We employed five such $\mathbf{q}$ vectors, which we believe supply a representative set of noncollinear excited states for a qualitative study of their role in thermodynamic properties.

Our main result is shown in Fig. 7 where the calculated temperature dependence of the magnetic contribution to the expansion coefficient, $\alpha(T)$, is presented for γ-Fe and Fe_3Pt. The coefficient $\alpha(T)$ was calculated as the derivative with respect to temperature of the average value of the specific volume $\langle v(T) \rangle$. The calculations were done with and without taking into account noncollinear states.

For γ-Fe in both approaches we obtain a large positive thermal expansion coefficient. This is completely different for Fe_3Pt, where accounting for noncollinear excitations changes the sign of the thermal expansion coefficient. It is seen that with the use of only collinear magnetic states the coefficient $\alpha(T)$ is positive at very low temperatures and nearly zero for higher temperatures. Inclusion of noncollinear configurations leads to a negative sign of $\alpha(T)$ over a wide temperature interval. The thermal expansion coefficient due to magnetic effects has been obtained experimentally for Fe_3Pt (Ref. 5) only. Its sign and order of magnitude are in agreement with our results, although the functional form, especially an experimental peak slightly below T_C, is not brought out by our calculations.

We can give a simple interpretation of these results using the information we have for the total energy, $E(v,m,\mathbf{q})$. Beginning with γ-Fe, we read off from Fig. 1 that the ground state is nonmagnetic. At finite temperatures the states with a finite local magnetic moment will be occupied. In Fig. 8 we show the distribution of the magnitude of local magnetic moments calculated with Eq. (25). Here with increasing temperature T the

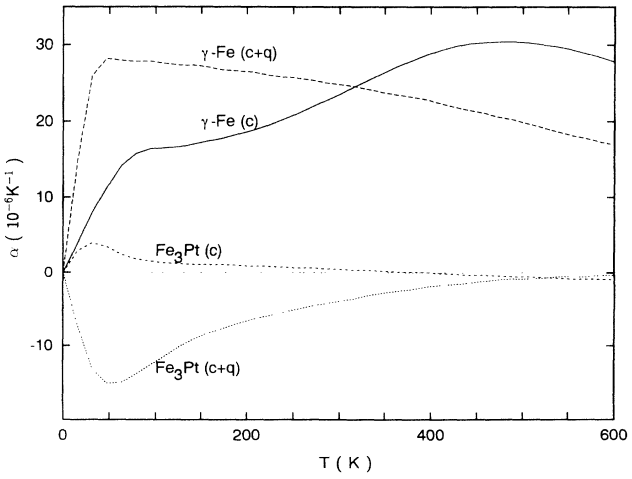

FIG. 7. Expansion coefficient α as a function of temperature T calculated for γ-Fe and Fe_3Pt; (I) using only collinear states (c) and (II) including collinear and noncollinear states ($c+q$).

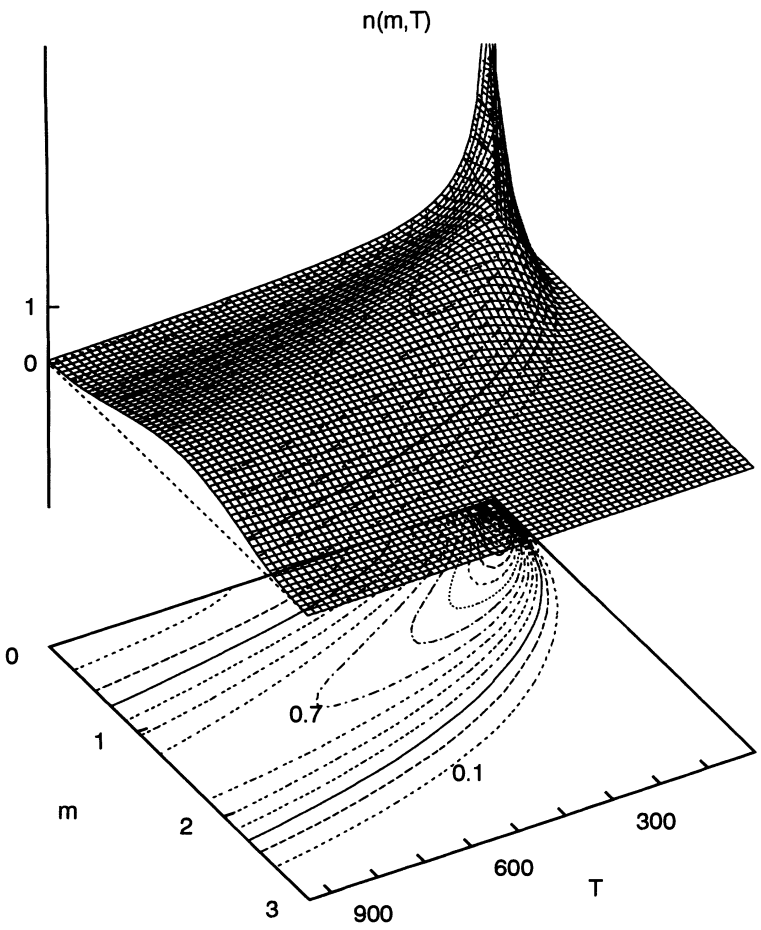

FIG. 8. Contours and surface of the distribution of magnetic moments, m, in μ_B with temperature T in K for γ-Fe.

maximum and, as a result, the average value of the distribution is shifted to larger values of m. However from the energy contours shown in Fig. 2 it becomes clear that an increase of the moment costs more energy for the states with smaller volume. Therefore the occupation of the states with larger volume increases faster than for the states with smaller volumes. This conclusion is valid for both calculational approaches, i.e., with and without including noncollinear states. Accounting for noncollinear states increases the number of magnetic excitations and leads to a faster increase of the average moment and correspondingly to a faster increase of the average volume.

We point out that γ-Fe does not exist as a stable phase at low temperatures and, therefore, for a comparison with experimental results one must take into account the state in which γ-Fe has been stabilized. However it is worth mentioning that our results are in agreement with recent experimental findings of Acet *et al.*[49]

The situation is different in Fe_3Pt. Here the ground state is ferromagnetic with an iron moment of $m_0 = 2.67\mu_B$. Therefore excited states can have both smaller magnetic moments, $m < m_0$, and larger magnetic moments, $m > m_0$, see Figs. 5 and 6. Let us first restrict our attention to collinear states only. In Fig. 5 one sees that low-energy excitations form energy contours which are almost symmetric with respect to the direction of variation of the parameters m and v. With increasing excitation energy the contours lose their symmetry and the states with smaller m and v increase slowest in energy making energetically preferable a decrease of the average values of m and v with heating. However, the factor m^2 in the integration formula, Eqs. (22) and (24), opposes this tendency and accounts for a larger number of states with larger m. Our calculations show that both effects almost compensate each other and for a wide temperature interval the value of the expansion coefficient is very small.

The inclusion of noncollinear states, Fig. 9, breaks the balance in favor of states with smaller moments and correspondingly smaller volumes. This is caused by the preferable occupation of noncollinear excited states with $m < m_0$ discussed in the previous section. Large occupation of noncollinear states with smaller values of m and v gives a negative magnetic contribution to the thermal expansion coefficient. A negative value of the magnetic contribution agrees with experiment and together with the usual positive thermal expansion leads to the Invar anomaly in Fe-Pt Invar alloys.

V. CONCLUSION

Our treatment of the electronic and magnetic properties of itinerant-electron systems presented here has

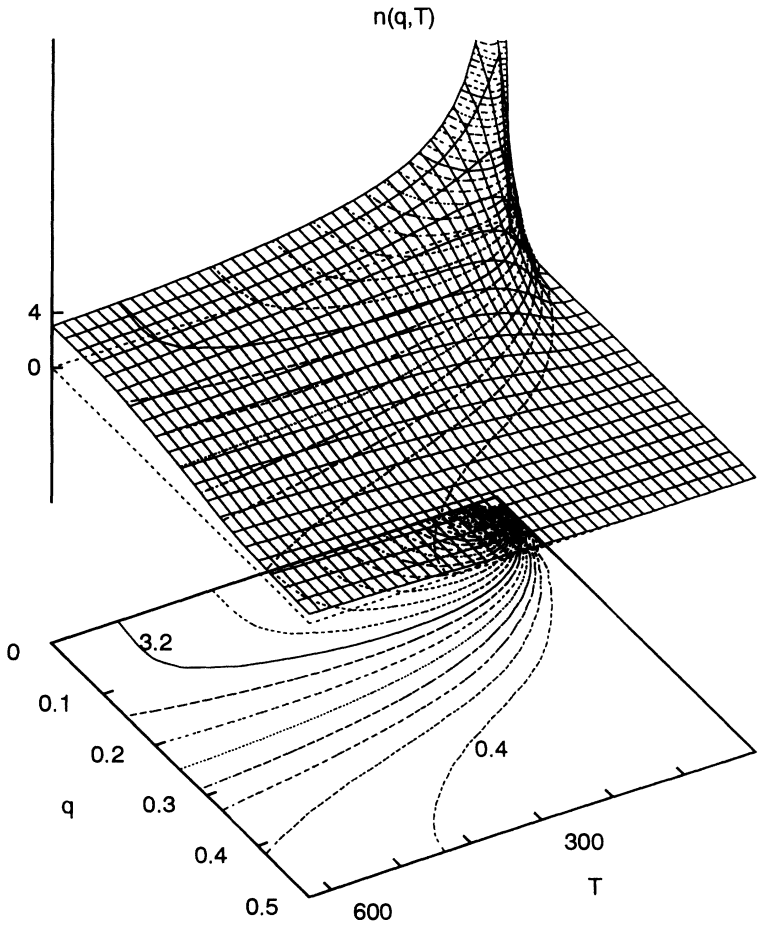

FIG. 9. Contours and surface of the distribution of the spiral vectors $\mathbf{q} = q(1,1,1)\frac{2\pi}{a}$ with temperature T in K for Fe_3Pt.

grown out of a long development connected with the work of Korenman, Heine, Moriya, and many others.[50–56,34] This is not the place to discuss the similarities and differences in our work compared with the many previous theories. Let it be said that Korenman *et al.*[57] treated the vector nature of the magnetic moments formed by the itinerant electrons like we do. But unlike Korenman's, our calculations are self-consistent concerning the charge and spin densities and the interatomic magnetic moment arrangements. We thus succeeded in describing the vector nature of the magnetic moments whose magnitude and direction are treated in a noncollinear constrained moment calculation as independent variables for an *ab initio* calculation of the total energy. This supplies the energetics of spin fluctuations and enabled us to make a step — although crude — in the direction of determining finite temperature properties.

Our calculations describe the magnetovolume properties of γ-Fe and Fe_3Pt. While the results for γ-Fe are not easily compared with experimental data, the results obtained for Fe_3Pt agree semiquantitatively with experimental facts, notably with the Invar behavior. On first sight it does not appear surprising that in Fe_3Pt with increasing temperature the magnetic moment and thus the specific volume decrease. One should bear in mind, however, that the decreasing magnetic moment is not the usual decreasing thermal average but is brought about by longitudinal spin fluctuations that are triggered by transverse fluctuations. These, in fact, in γ-Fe cause the nonintuitive initial increase of the magnetic moment when the temperature increases and thus lead to an anomalously large thermal expansion here.

ACKNOWLEDGMENT

This work was partially supported by the Deutsche Forschungsgemeinschaft through SFB 252 Darmstadt, Frankfurt, Mainz.

[1] C.E. Guillaume, C.R. Acad. Sci. **125**, 235 (1897).
[2] E.F. Wassermann, Phys. Scr. **T25**, 209 (1989).
[3] E.F. Wassermann, in *Ferromagnetic Materials,* edited by K.H.J. Buschow and E.P. Wohlfarth (North-Holland, Amsterdam, 1990), Vol. 5.
[4] A.Z. Menshikov, Physica B **161**, 1 (1989).
[5] N.L. Sedov, *Antiferromagnetism Gamma-Shelesa / Problema Invara* (Nauka Gl. Red. Fis.-Mat. Lit., Moscow,

1987).
[6] I.A. Campbell and G. Creuzet, in *Metallic Magnetism,* edited by H. Capellmann (Springer, Berlin, 1987).
[7] A.R. Williams, V.L. Moruzzi, C.D. Gelatt, Jr., J. Kübler, and K. Schwarz, J. Appl. Phys. **53**, 2019 (1982).
[8] A.R. Williams, V.L. Moruzzi, C.D. Gelatt, Jr., and J. Kübler, J. Magn. Magn. Mater. **31-34**, 88 (1983).
[9] R.J. Weiss, Proc. Phys. Soc. **82**, 281 (1963).
[10] P. Mohn, K. Schwarz, and D. Wagner, Physica B **161**, 153 (1989).
[11] D. Wagner, J. Phys. Condens. Matter **1**, 4635 (1989).
[12] P. Entel and M. Schröter, Physica B **161**, 160 (1989).
[13] E.G. Moroni and T. Jarlborg, Physica B **161**, 115 (1989).
[14] E.G. Moroni and T. Jarlborg, Phys. Rev. B **41**, 9600 (1990).
[15] H.J. Gerber, K.D. Usadel, and G. Brieskorn, Physica B **161**, 157 (1989).
[16] M.U. Luchini, V. Heine, and G.J. McMullan, J. Phys. Condens. Matter **3**, 8647 (1991).
[17] M. Podgorny, Phys. Rev. B **43**, 11300 (1991).
[18] M. Podgorny, Phys. Rev. B **46**, 6293 (1992).
[19] M. Podgorny, M. Thon, and D. Wagner, J. Magn. Magn. Mater. **104-107**, 703 (1992).
[20] P. Entel, E. Hoffmann, P. Mohn, K. Schwarz, and V.L. Moruzzi, Phys. Rev. B **47**, 8706 (1993).
[21] W. Kohn and L.J. Sham, Phys. Rev. A **140**, 1133 (1965).
[22] U. von Barth and L. Hedin, J. Phys. C **5**, 1629 (1972).
[23] J. Sticht, K.-H. Höck, and J. Kübler, J. Phys. Condens. Matter **1**, 8155 (1989).
[24] L.M. Sandratskii, Phys. Status Solidi B **135**, 167 (1986).
[25] L.M. Sandratskii, Solid State Commun. **75**, 527 (1990).
[26] M. Uhl, L.M. Sandratskii, and J. Kübler, J. Magn. Magn. Mater. **103**, 314 (1992).
[27] V.L. Moruzzi, Phys. Rev. B **41**, 6939 (1990).
[28] C. Herring, in *Magnetism IV*, edited by G. Rado and H. Suhl (Academic Press, New York, 1966).
[29] A.R. Williams, J. Kübler, and C.D. Gelatt, Jr., Phys. Rev. B **19**, 6094 (1979).
[30] J. Kübler and V. Eyert, in *Electronic and Magnetic Properties of Metals and Ceramics*, edited by K.H.J. Buschow (VCH Verlagsgesellschaft, Weinheim, 1991).
[31] A.R. Williams, V.L. Moruzzi, J. Kübler, and K. Schwarz, Bull. Am. Phys. Soc. **29**, 278 (1984).
[32] V.L. Moruzzi, P.M. Marcus, K. Schwarz, and P. Mohn, Phys. Rev. B **34**, 1784 (1986).
[33] P.H. Dederichs, S. Blügel, R. Zeller, and H. Akai, Phys. Rev. Lett. **53**, 2512 (1984).
[34] L.M. Sandratskii and P.G. Guletskii, J. Magn. Magn. Mater. **79**, 306 (1989).
[35] L.M. Sandratskii and J. Kübler, Phys. Rev. B **47**, 5854 (1993).
[36] O.N. Mryasov, A.I. Liechtenstein, L.M. Sandratskii, and V.A. Gubanov, J. Phys. Condens. Matter **3**, 7683 (1991).
[37] O.N. Mryasov, V.A. Gubanov, and A.I. Liechtenstein, Phys. Rev. B **45**, 12330 (1992).
[38] K. Schwarz and P. Mohn, J. Phys. F **14**, L129 (1984).
[39] J. Kübler, Phys. Lett. A **81**, 81 (1981).
[40] C.S. Wang, B.M. Klein, and H. Krakauer, Phys. Rev. Lett. **54**, 1852 (1985).
[41] Y. Tsunoda, J. Phys. Condens. Matter **1**, 10427 (1989).
[42] Y. Tsunoda, Prog. Theor. Phys. Suppl. **101**, 133 (1990).
[43] L.M. Sandratskii and J. Kübler, J. Phys. Condens. Matter, **4**, 6927 (1992).
[44] J. Hesse, G. Nölle, and H. Körner, Solid State Commun. **46**, 721 (1983).
[45] M. Shimizu, Rep. Prog. Phys **44**, 329 (1981).
[46] K. Sumiyama, M. Shiga, Y. Kobayashi, K. Nishi, and Y. Nakamura, J. Phys. F **8**, 1281 (1978).
[47] A.J. Holden and M.V. You, J. Phys. F **12**, 195 (1982).
[48] Y. Ishikawa, K. Tajima, Y. Noda, and N. Wakabayashi, J. Phys. Soc. Jpn. **48**, 1097 (1980).
[49] M. Acet, H. Zähres, E.F. Wassermann, and W. Pepperhoff, Phys. Rev. B **49**, 6012 (1994).
[50] V. Korenman, J.L. Murray, and R.E. Prange, Phys. Rev. B **16**, 4032 (1977).
[51] T. Moriya, J. Magn. Magn. Mater. **14**, 1 (1979).
[52] M.V. You and V. Heine, J. Phys. F **12**, 177 (1982).
[53] T. Oguchi, K. Terakura, and N. Hamada, J. Phys. F **13**, 145 (1983).
[54] A.J. Pindor, J. Staunton, G.M. Stocks, and H. Winter, J. Phys. F **13**, 979 (1983).
[55] B.L. Gyorffy, A.J. Pindor, J. Staunton, G.M. Stocks, and H. Winter, J. Phys. F **15**, 1337 (1985).
[56] A.I. Liechtenstein, M.I. Katsnelson, V.P. Antropov, and V.A. Gubanov, J. Magn. Magn. Mater. **67**, 65 (1987).
[57] V. Korenman, in *Metallic Magnetism*, edited by H. Capellmann (Springer, Berlin, 1987).